Electronic Supplementary Material (ESI) for Nanoscale.
This journal is © The Royal Society of Chemistry 2023

SUPPLEMENTARY INFORMATION

Supplementary materials and methods

Key resources table

REAGENT or RESOURCE	SOURCE	IDENTIFIER
Antibodies		
Rabbit polyclonal anti-β-tubulin III	Sigma-Aldrich	T2200
Mouse monoclonal anti-PSD95	Invitrogen	MA1-045
Guinea pig anti-vesicular glutamate transporter 1	Sigma-Aldrich	AB5905
Alexa Fluor 405 goat anti-rabbit	Invitrogen	A-31556
Alexa Fluor 594 goat anti-mouse	Invitrogen	A-11005
Alexa Fluor 488 goat anti-guinea pig	Invitrogen	A-11073
FM1-43	Molecular Probes, Life Technology	T3163
Chemicals		
Potassium dichromate	Sigma-Aldrich	483044
Potassium chromate	Sigma-Aldrich	529508
Mercuric chloride	Sigma-Aldrich	215465
Sucrose	Sigma-Aldrich	S7903
Quick-hardening mounting medium	Eukitt, Sigma-Aldrich	03989
NaCl	Sigma-Aldrich	S7653
NaHCO	Sigma-Aldrich	S5761
HEPES	Sigma-Aldrich	102453336
KCl	Sigma-Aldrich	P9541
$CaCl_2$	Sigma-Aldrich	C7902
MgSO4	Carlo Erba	459667
$NaPO_4H_2$	Sigma-Aldrich	S5011
Poly-L-ornithine	Sigma-Aldrich	P4957
Neurobasal A Medium	Invitrogen	10888022
B27 supplement	Thermofisher	17504-044
Paraformaldehyde	Sigma-Aldrich	158127
Glycine	Sigma-Aldrich	GE17-1323-01
PBS	Sigma-Aldrich	1003393914
Fetal bovine serum	Life Technology	10500064
Bovine serum albumin	Sigma-Aldrich	A4503
Triton-X 100	Sigma-Aldrich	T8787
Mounting medium	Fluoromount, Sigma-Aldrich	00-4958-02
K Gluconate	Sigma-Aldrich	G4500
EGTA	Sigma-Aldrich	324626
$MgCl_2$	Sigma-Aldrich	M2670
Na_2ATP	Sigma-Aldrich	A7699
Glucose	Sigma-Aldrich	G7528

Normal goat serum	Thermofisher	10000C
Experimental Models: Organisms/Strains		
Rat: Wistar	Envigo	16806M
Drugs		
Ketamine	Ketamine Imalgene®, Merial Laboratories	6740-88-1
Xylazine	Sedaxylan®, Dechra Veterinary Products	08714225150571
Glutamate	Sigma-Aldrich	G1501
TTX	Hellobio	HB1034
Gabazine	Sigma-Aldrich	S106
Software		
XPloRat	Tejada et al., 2018	Version 1.1.0, 2005
EthoVision XT	Noldus	Version XT 16
RECONSTRUCT	Risher et al., 2014	Version 1.1.0.0, 2007
Volocity software	Perkin Elmer	Version 6.3
Multiclamp 700A	Axon CNS, Molecular Devices	Version 1.3.0.05
pClamp	Molecular Devices	Version 10
AxoGraph X	Axograph Scientific	Version 1.7
HCImage Live	Hamamatsu Photonics	U11158
Fiji	Rauti R. et al., 2016	Version 1.53c
Other		
Cat collar	Camon	8019808087276
Biopsy punch	Quagen unicore, Sigma- Aldrich	WHAWB100073

Graphene oxide nanosheets synthesis and characterization. The specific batch of GO nanosheets used here, already reported in[1], was thin (1-2 carbon layers) and of a few hundred nanometers in lateral dimension (95% < 475 nm), with reproducibly demonstrated biocompatibility and purity (Supp. Fig 1). *Biological-grade s-GO* was synthesized from graphite powder (Sigma Aldrich, UK) by the modified Hummers method as previously described, under endotoxin-free conditions[2]. Briefly, sulfuric acid is added to the mixture of the reaction containing graphite and sodium nitrate. Then, potassium permanganate is added very slowly. After 30 min, water for injection is transferred slowly and the reaction is kept at 98°C for 30 min. Afterwards, hydrogen peroxide is added to stop the reaction. The consequent GO purification was performed by centrifugation steps until the pH of the supernatant was neutral. s-GO material was obtained after 5 min sonication and then purified by centrifugation[3]. *Atomic force microscopy (AFM)* - An Asylum MFP-3D atomic force microscope (Oxford instruments) operating in standard air-tapping mode and equipped with silicon probes (Ted Pella) with a resonance frequency of 300 kHZ and a nominal force of 40 N/m was used to characterize the

surface. Images were processed using Gwyddion software (v. 2.56). *Scanning electron microscopy (SEM)* - SEM images were recorded on a Magellan 400L field emission scanning electron microscope (Oxford instruments) at the ICN2 Electron Microscopy Unit, which was equipped with an Everhart-Thornley as secondary electrons detector and using an acceleration voltage of 20 kV and beam current of 0.1 nA. The sample was deposited on an Ultrathin C on Lacey C grid, any excess of material was removed and dried overnight at room temperature. *UV-Vis spectroscopy* - Absorbance was evaluated by using a Nanodrop 2000c spectrophotometer (Thermo Scientific) at room temperature using a Hellma QS Quartz micro cuvette. GO samples were prepared in water in a concentration range of 2.5-20 μg/mL. *Raman spectroscopy* - Raman spectra were acquired with a confocal Raman microscope (Witec) at room temperature coupled to 633 nm laser excitation and using a grating of 600 g/nm. Single Raman spectra were collected on several spots after irradiation with a power of 1 mW for 10 s and using a 50x objective to focus on the sample. *Zeta potential measurements***.** Zeta potential (ζ) was measured by a Zeta-sizer Nano ZS (Malvern instruments) equipped with disposable capillary cells at the ICN2 Molecular Spectroscopy and Optical Microscopy Facility. *X-ray photoemission spectroscopy (XPS)* **-** XPS data was obtained using a Phoibos 150 (SPECS, GmbH) electron spectrometer equipped with a hemispherical analyzer, operating under ultrahigh-vacuum conditions, and with an Al Kα (hν = 1486.74 eV) X-ray source, at the ICN2 Photoemission Spectroscopy Facility. In order to estimate the photoelectron peak intensities CasaXPS software was used.

The in vivo PTSD model and design of treatments. Male adult Wistar rats weighed 230-280 g (n = 20) were used to perform the *in vivo* experiments. Food and water were provided at libitum. The enclosure was maintained at 21 ± 2 °C on a light-dark cycle (lights on from 7 p.m. to 7 a.m.). Behavioral experiments were performed as described previously[4]. Briefly, aversive memory behavioral responses were evaluated in the avoidance box, which consisted of a rectangular arena (40 × 26 × 36 cm) with black acrylic-plexiglass walls covered with a transparent plexiglass lid. At one side of the arena, an alligator clip fixed in the wall is positioned 4 cm above the floor. A smaller box (20 × 26 × 22 cm) covered with a black plexiglass lid, named hide box, is positioned in the opposite direction of the rectangular arena. Arena and hide box were separated by a small 6 × 6 cm square hole allowing free access to both chambers. Rats were placed inside the hide box with free access to the arena for 3 consecutive days to habituate to the apparatus during 10 minutes. On the fourth day, the time spent in the following defensive

behavior was recorded: head out (namely, the rat scanning the environment from a protected position, measured as poking of the head, or of head and shoulders, outside of the hide box, but with the bulk of the rat body inside of it). Next, rats were divided in two groups (n = 4 for UC and n = 6 for WC), exposed to either a piece (2 cm) of an unworn collar (UC), without any cat odor or a piece of the collar previously worn by the cat, named worn collar (WC). Collars were worn by an encaged cat. Rats were re-exposed (10 minutes) to the context, arena without the cat collar to evaluate the aversive memory related to the contextual conditioned fear. Head out behavioral response was analyzed during the re-exposure to the context at 8 days post-exposure. Shortly thereafter, long-term anxiety-related behavior was evaluated using the EPM. Which consisted of four arms (50 × 10 × 40 cm), two open arms (without walls) and two closed arms (with 40 cm high walls) connected by a central square (10 × 10 cm). The maze was elevated 50 cm from the ground. Rats (n = 4 for UC and n = 6 for WC) were placed in the closed arm and were allowed to freely explore the apparatus for 5 minutes. Percentage of time spent in the open zone was evaluated.

Exploratory and locomotor activities of rats (n = 4 for UC and n = 6 for WC) were measured in the OF apparatus, a square arena with the 60 × 60 × 40 cm black plexiglass walls and floor. Total distance moved (cm) in the OF were analyzed, following the EPM testing. All behavioral tests were performed between 8 a.m. and 12 p.m. under 40 lx luminosity and videorecorded for off-line analysis. The XPloRat[5] and EthoVision XT (Noldus, The Netherlands) software were used to score the behaviors. Next day, animals were submitted to stereotaxic surgery as described previously[6]. Briefly, animals were anesthetized with intraperitoneal injection of ketamine (Ketamine Imalgene®, Merial Laboratories) and xylazine (Sedaxylan®, Dechra Veterinary Products) at 92 mg/kg and 10 mg/kg body weight, respectively, and fixed in a stereotaxic frame. A stainless-steel guide cannula (outer diameter, 0.6 mm, and inner diameter, 0.4 mm) was implanted in the diencephalon aimed to the LA. The upper incisor bar was set at 3.3 mm below the interaural line so that the skull was horizontal between bregma and lambda. The guide cannula was vertically introduced using bregma as the reference and the following coordinates: A.P.−3.48 mm, M.L.−5.2 mm and D.V.−7 mm, according to[4]. At the end of the surgery, the acrylic resin and two stainless steel screws were used to fix the guide cannula to the skull. In order to protect the guide cannula from obstruction a stainless-steel wire was used to seal it. Analgesic and antibiotic medications were administrated postoperatively. Three days later, rats

were gently wrapped in a cloth and held while they received a random treatment into LA of either s-GO (50 μg/mL) or ACSF solution (composition described below) delivered by a needle (0.3 mm of outer diameter) linked to a syringe (Hamilton) through a polyethylene tube. The injection needle was inserted through the guide-cannula until it reached the LA (2 mm below the guide-cannula). Only rats that needle tip reached the LA were included in the study. Four days later, animals were submitted to the behavioral testing. All experimental procedures were planned to minimize the number of animals used and their suffering.

Golgi-cox staining and dendritic spine analysis. After behavioral experiments, rats (n = 20) were anaesthetized as described above and decapitated, their brains were collected and prepared to the Golgi-Cox staining protocol[7]. Briefly, brains were incubated in the Golgi-Cox solution (1 % potassium dichromate, 0.8 % potassium chromate and 1 % mercuric chloride) in the dark at room temperature (RT) for 25 days. After that, brains were incubated in sucrose solution at 30 % for 48 hours and sliced in coronal sections (200 μm thickness) at the level of the amygdala using a vibratome (Leica VT100S). Brain slices were mounted onto microscope slides with Eukitt Quick-hardening mounting medium (Sigma-Aldrich). Histological sections were analyzed and images stacks of the LA neurons were acquired using a Leica DM6000 upright confocal microscope with a 63× oil immersion objective. The serial section images were aligned, and dendritic spines of pyramidal neurons were subjected to blind analysis[8] in RECONSTRUCT software (http://synapses.clm.utexas.edu/tools/reconstruct/reconstruct.stm; RID:SCR_002716). Primary and secondary dendrite, defined as any branch emerging from the soma and branch emerging from a primary dendrite, respectively, with a length of 40 μm from its origin was analysed[9,10]. All dendrite protrusions were considered as spines, regardless to their morphological characteristics.

In vitro dissociated amygdala cultures. Primary cultures of amygdala cells were obtained from postnatal (P 7-10) juvenile Wistar rats and prepared as previously described[4] with slight modifications. In brief, rat brains were quickly removed from the skull and placed in fresh ice-cold artificial cerebrospinal fluid (ACSF) containing (in mM): 124 NaCl, 24 $NaHCO_3$, 13 glucose, 5 HEPES, 2.5 KCl, 2 $CaCl_2$, 2 $MgSO_4$ and 1,2 $NaPO_4H_2$ with a pH of 7.3-7.4 when saturated with 95 % O_2 and 5 % CO_2[11]. Coronal brain sections were cut using a vibratome (LeicaVT1000S) and under a dissecting microscope (Olympus SZ40), the regions containing the amygdala complex was visually identified following defined anatomical coordinates: Bregma -

1.8 mm, - 2.4 mm and 2.8 mm[12]. Using a biopsy punch with a diameter of 1 mm (Kai Medical, Japan) the amygdala tissue was collected to be enzymatically and mechanically dissociated following standard protocol[13]. Cells were seeded onto poly-L-ornithine-coated glass coverslips at a density of 1000 cells/mm^2 and maintained in controlled conditions (at 37 °C, 5 % CO^2) for 8–12 days *in vitro* (DIV) prior to experiments in Neurobasal A Medium (Invitrogen) containing B27 supplement (Thermofisher).

Immunohistochemistry and confocal microscopy. Cultured amygdala neurons (5 cultures; 8-12 DIV) were fixed by 4 % formaldehyde (prepared from fresh paraformaldehyde, PFA; Sigma) in PBS at RT. After 15 min in glycine 0.3 M in PBS, cells were blocked and permeabilized in 10 % fetal bovine serum (FBS), 3 % bovine serum albumin (BSA), 0.3 % Triton-X 100 in PBS (blocking solution) for 30 min at RT. As primary antibodies, we used rabbit polyclonal anti-β-tubulin III (Sigma-Aldrich, 1:500 dilution), mouse monoclonal anti-PSD95 (Invitrogen, 1:400 dilution), and guinea pig anti-vesicular glutamate transporter 1 (VGlut1; Sigma-Aldrich, 1:1000), diluted in the blocking solution for 60 min at RT. As secondary antibodies, we used Alexa 405 goat anti-rabbit (Invitrogen, dilution 1:500), Alexa 594 goat anti-mouse (Invitrogen, dilution 1:500), and Alexa 488 goat anti-guinea pig (Invitrogen, 1:500) diluted in normal goat serum (NGS) 5 % in PBS for 45 min at RT. Finally, cells were mounted on 1 mm thick glass coverslips using the Fluoromount mounting medium (Sigma-Aldrich). To quantify VGlut1 and PSD95 puncta, $n = 50 \pm 10$ *z*-stacks (acquired every 0.15 μm) were taken from $n = 5$ randomly selected fields (70.64 μm × 70.64 μm) per coverslip using a Nikon C2 Confocal, equipped with Ar/Kr, He/Ne, and UV lasers. Images were acquired with a 60× (1.4 NA) oil-objective (using oil mounting medium, 1.515 refractive index). We selected only VGlut1-positive and PSD95-positive puncta (≥0.1-0.8≥ μm^3) co-localized with β-tubulin III-positive signal in 6 different ROIs (32.9 μm × 8.9 μm) per image containing one or more distal neurites. For each image, VGlut1 puncta were normalized to the β-tubulin III positive volume. Images were analyzed using the Volocity software (Perkin Elmer).

Electrophysiology. Input resistance and cells capacitance were measured online with the membrane test feature of the pClamp software. Spontaneous activity was recorded in voltage clamp mode at a holding potential of −58 mV, not corrected for the liquid junction potential which was −12 mV (calculated with the Clampex software; Molecular Devices, Sunnyvale, CA, USA). The stability of the patch was repetitively monitored during the experiments by checking

the input and series resistance. Cells exhibiting 15 % changes were excluded from the analysis. The series resistance was <20 MΩ and it was not compensated. Input resistance and cells capacitance were measured online with the membrane test feature of the pClamp software.

To induce LTP in dissociated cultures under voltage clamp mode, our previously described protocol was applied[4]. Briefly, after recording spontaneous activity for 8 min as baseline, 50 μM of glutamate for 30 s was applied, while the membrane potential of the recorded cell was depolarized from -58 mV to +4 mV. In the experiments where dissociated cells were treated with s-GO, it was applied at a concentration of 20 μg/mL for 30 s through the perfusion system, alone or in combination with 50 μM of glutamate.

The effects of LTP induction and s-GO interference were monitored for 24 min after the baseline collection. mPSC were recorded in the presence of TTX (1 μM) to block fast voltage-dependent sodium channels. Analyzing mPSCs' features (i.e., frequency and amplitude) provides a valuable tool to hints at functional and structural changes in pre- and postsynaptic mechanisms of CNS synapses implicated in neurotransmission homeostasis and plasticity. mPSCs were analyzed offline using the software AxoGraph X (Axograph Scientific), which exploits a detection algorithm based on a sliding template. Templates characterized by diverse decay times (τ) were used to separate offline glutamate AMPA-receptor mediated postsynaptic currents (τ ~3 ms) and those mediated by $GABA_A$ -receptors (τ ~20 ms). For each recording, all the collected events were averaged, and the peak amplitude and kinetic properties of the mean current were measured. The averaged values of sPSC and mPSC were calculated between 18 and 24 min after LTP induction and normalized for the pre-treatment baseline values.

In paired recordings, monosynaptically connected glutamatergic neurons, recorded in the presence of gabazine (10 μM) were recognized by the short latency (<3 ms)[14,15] between the peak of the presynaptic neuron and the onset of eEPSC. The presynaptic neuron in current clamp mode was held at -70 mV (by ≤ 0.02 nA negative current injection), and action potentials were evoked by delivering short (4 ms) positive (1 nA) square current pulses. To characterize the short-term dynamics of synaptic contacts as well as changes in the p_r from the presynaptic neurons, we delivered to presynaptic neurons repeated paired pulse stimulation at 20 Hz (every 20 s; 6 times that were pooled together and averaged). We estimated the p_r of glutamatergic amygdala synapses by quantifying the PPR (calculating the ratio between the mean peak amplitude of the second and the first eEPSC[41,42]) and we assessed changes in p_r by monitoring

the PPR up to 24 min after different treatments. The averaged values of PPR were calculated between 18 and 24 min after treatment and normalized for the pre-treatment baseline values. Glutamate-induced inward currents were assessed by a 30 s-long application of glutamate (50 μM) in the presence of TTX 1 μM and the area under the current was measured through the pClamp software.

FM1-43 Imaging. Depolarization-dependent staining of synaptic terminals with the styryl dye N-(3-triethylammoniumpropyl)- 4-(4-(dibutylamino)styryl)pyridinium dibromide (FM1-43, Molecular Probes, Life Technology) was obtained by incubating amygdala cultures (after 10 min saline buffer wash at RT) for 2 min with 2 mL of extracellular recording solution containing 50 mM KCl and 15 μM FM1–43 dye. Next, this buffer was replaced with 2 mL of extracellular recording solution containing FM1-43, and cells were left to recover for 10 min to ensure complete recycling of the vesicles[14]. Cells were then incubated for 10 min with TTX (1 μM) to prevent network activity altering the rate of FM release. After loading with FM1-43 dye, cultures were treated with 50 μM of Glutamate, in the presence or absence of 20 μg/mL of s-GO or with saline for 30 s at RT. As further control we treated cultures with s-GO only. For live imaging, cultures were transferred to the stage of a Nikon Eclipse Ti−U inverted microscope where they were continuously perfused (5 mL/minute) at RT with the extracellular recording solution containing TTX (1 μM). FM1-43-loaded cells were recorded with a 40× objective (PlanFluor, 0.60 NA) and excited at 488 nm with a mercury short lamp (Osram, Munich, Germany). Excitation light was separated from the light emitted from the specimens using a 395 nm dichroic mirror and DN filter (1/32). Images were constantly acquired at 7 fps every 150 ms using an ORCA-Flash4.0 V2 sCMOS camera (Hamamatsu Photonics, Japan) with a spatial resolution of 512 × 512 pixels. The set-up was controlled by HCImage Live software. After a basal recording (2 min), application of 50 mM KCl (2 min), followed by a 2 min of washout, was used to stimulate vesicle exocytosis from the dye-containing terminals, measured as a fluorescence loss. Offline analysis was performed on the image sequence with the image processing package Fiji[14]. After background subtraction, time-dependent fluorescence changes on FM1–43 labelled terminals were obtained by drawing regions of interest (ROIs) around fluorescent spots (typically 6 × 6 pixels in diameter drawn on neural processes), including as little background as possible. Corresponding tracings were transferred to Clampfit software (pClamp suite, 10.6 version; Molecular Device LLC, US) and the τ was measured from averaged

traces by fitting it with a mono-exponential function ($f(t)=\sum_{i=1}^{n} A_i e^{-t/\tau_i} + C$). To avoid imaging nonselective FM staining, only puncta that showed stimulus-dependent destaining were included in the analyse[14].

A

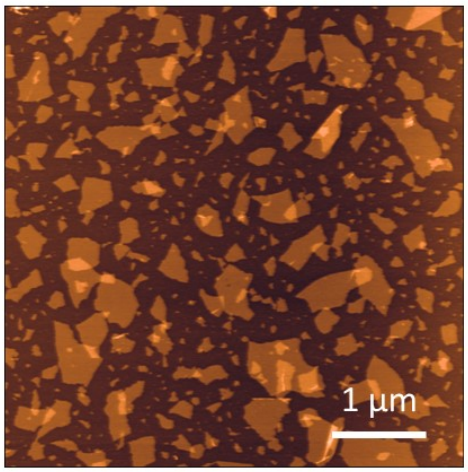

B

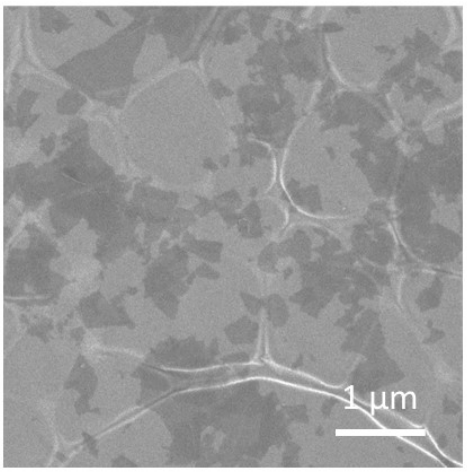

C

Physicochemical properties	***Technique***	***s-GO***
Lateral dimension	*AFM*	25 nm -1.5 µm (95% < 475 nm)
	SEM	50 nm -1.9 µm (95% < 850 nm)
Thickness	*AFM*	1 - 2 nm
Optical properties	*UV-Vis spectroscopy*	A_{230}= 0.053 * C_{GO} (µg/mL)
Degree of defects (I_D/I_G)	*Raman spectroscopy*	1.14 ± 0.03
Surface charge	*ζ-Potential*	-52.1 ± 0.4 mV
Chemical Composition (Purity)	*XPS*	*C: 72.2 %, O: 25.0 %, S: 1.2 %, B: 1.6 % (97.2%)*

Supplementary Figure 1. *Characterization of s-GO sheets.* (**A**) Height AFM image (dimension: 5x5; scale bar: 1 µm). (**B**) SEM micrograph (scale bar: 1 µm). (**C**) Summary of physicochemical properties by different analytical, spectroscopic, and microscopic techniques.

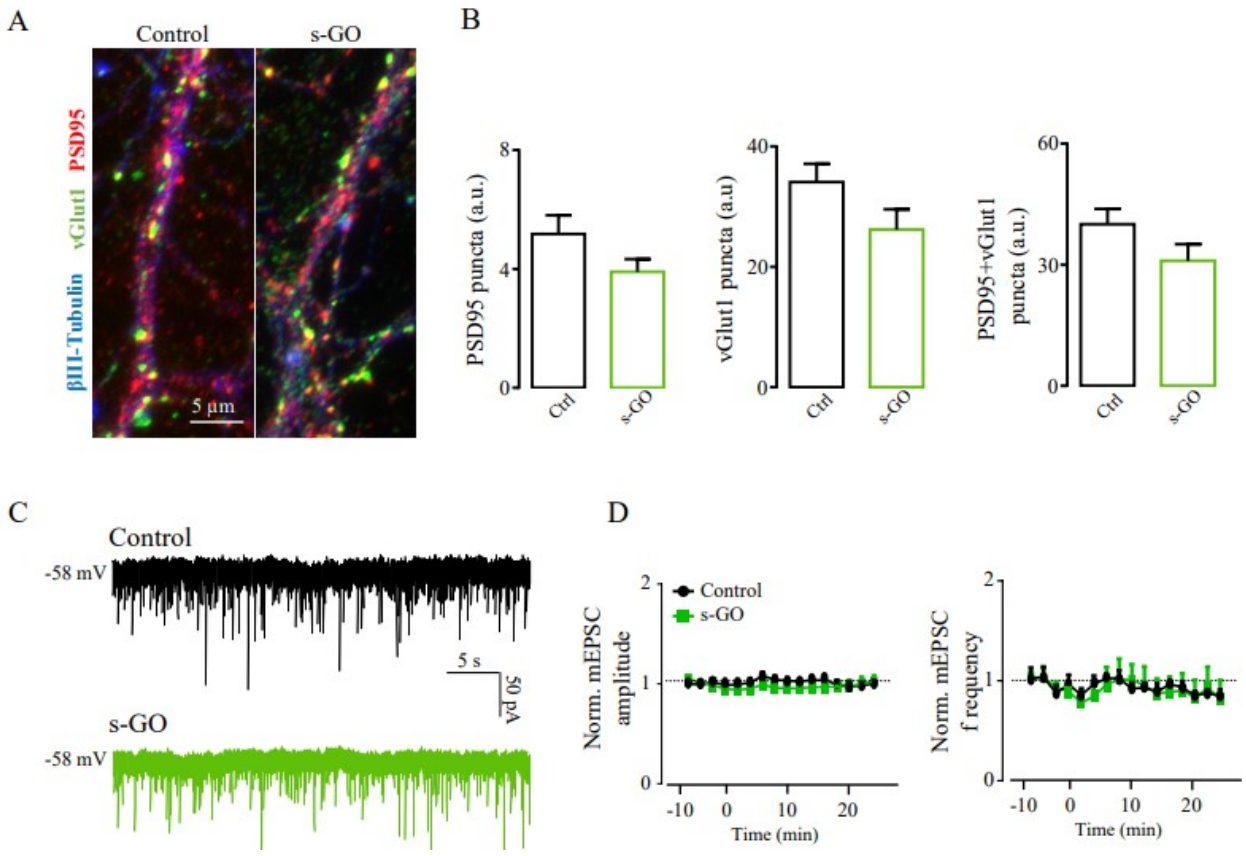

Supplementary Figure 2. *s-GO does not alter the amygdala synapses in control conditions.* (A) Confocal images of β-tubulin III positive (in blue) amygdala neurites co-labelled with the presynaptic (Vglut1, in green) and the postsynaptic (PSD95, in red) markers, in saline (right) or upon s-GO exposure (30 s; left). (B) Bar plots of the density of PSD95 puncta (5.2 ± 0.6 a.u. in control and 3.9 ± 0.4 a.u. in s-GO, n= 15 fields, 3 cultures each; p = 0.102), of VGlut1 puncta (34.1 ± 3.0 a.u. in control and 26.2 ± 3.3 a.u. in s-GO, n= 15 fields, 3 cultures each; p = 0.09), and of PSD95 + VGlut1 co-localization puncta (40.1 ± 3.8 a.u. in control and 31.0 ± 4.1 a.u. in s-GO, n= 15 fields, 3 cultures each; p = 0.114). (C) mPSC traces recorded 24 min after saline (30 s, black trace) or after 20 µg/mL s-GO (30 s, green trace). (D) Plots of the normalized mEPSC amplitude (right, 0.98 ± 0.03 in controls, n = 7, and 0.99 ± 0.06 in s-GO, n = 8; p =0.920, 24 min) and frequency (left, 0.88 ± 0.04 in controls, n =7, and 0.87 ± 0.18 in s-GO, n = 8; p = 0.903, 24 min) showing no effect upon s-GO treatment (30 s).

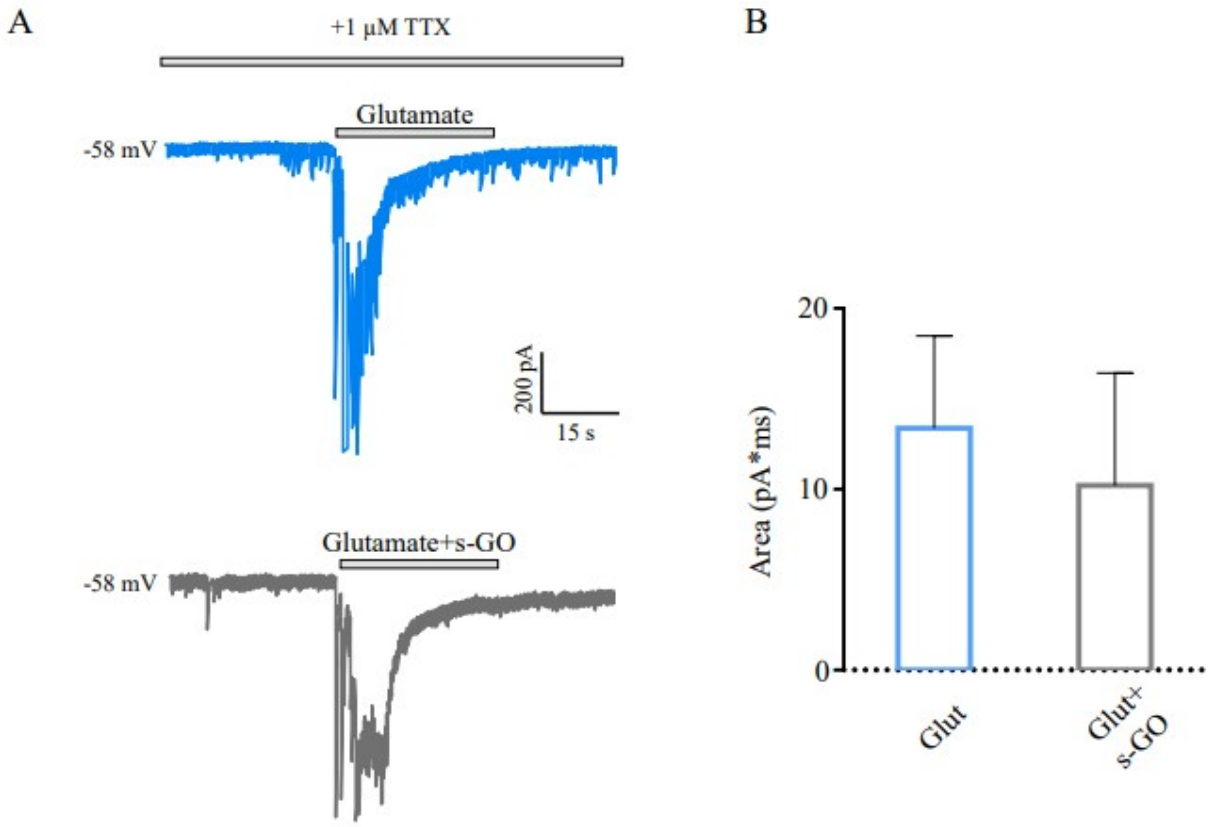

Supplementary Figure 3. *s-GO does not affect either the activity of postsynaptic glutamatergic receptors or the exogenously applied glutamate.* (A) The application of 50 µM glutamate activated glutamatergic receptor-mediated inward currents, independently from the presence of s-GO. (C) Bar plot illustrating the similar area of the glutamate-induced inward current with or without s-GO (13.36 ± 5.10 pA*ms in control, n =12, and 10.20 ± 6.21 in s-GO, n = 10; $p > 0.05$).

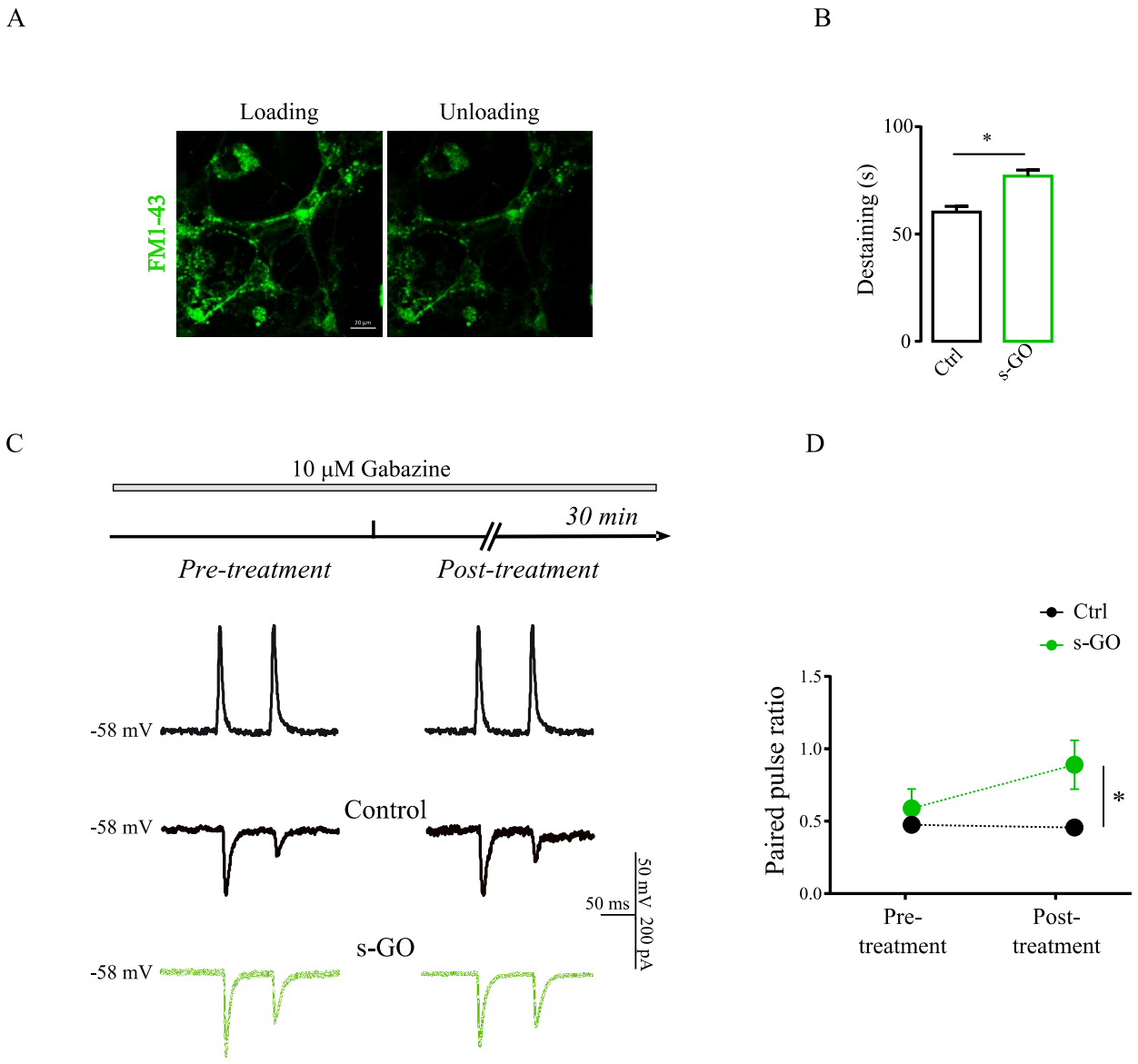

Supplementary Figure 4. *s-GO and vesicle release dynamics in control amygdala neurons.* (A) Fluorescence snapshots of FM1-43 loading (right) and unloading (left). (B) The histogram summarizes the τ values of FM1-43 destaining upon saline or s-GO (30 s; 60.27 ± 2.66 s in control, n=80 terminals, and 76.95 ± 2.87 s in s-GO, n=80 terminals, $p < 0.0001$). (C) Sketch of the experimental procedure (top) and representative traces of pair recordings (bottom). In the first row, presynaptic action potentials and below the corresponding unitary eEPSC, prior (left) and after (24 min, right) treatment with saline (control, black traces) or 20 ug/mL s-GO (s-GO, green traces). (D-E) The plot summarizes the averaged paired-pulse ratio measured prior and after (24 min) each

treatment. These were respectively 0.47 ± 0.06 and 0.46 ± 0.04 in control, 0.59 ± 0.13 and 0.89 ± 0.17 for s-GO; *p < 0.05.

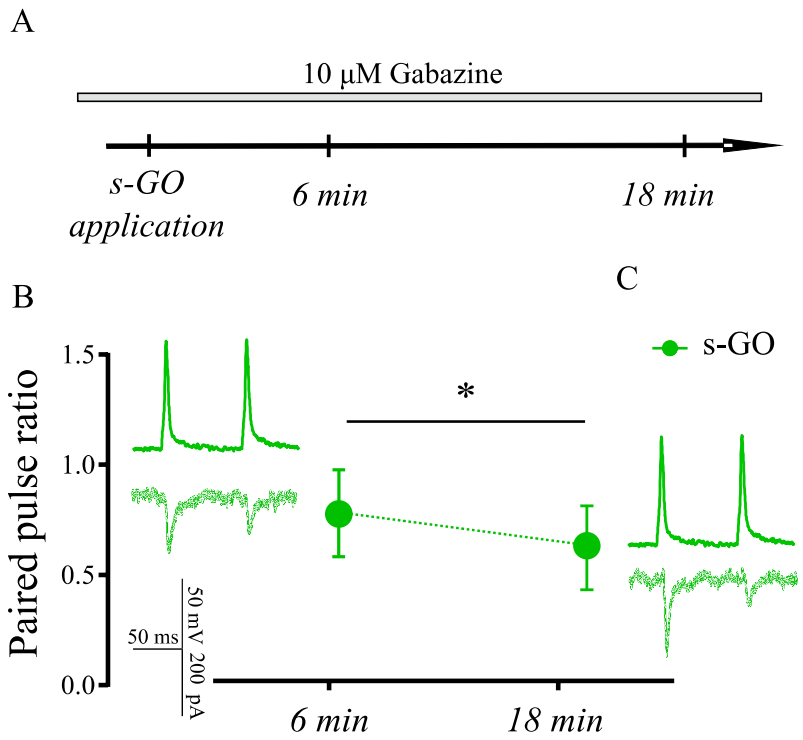

Supplementary Figure 5. *s-GO modulatory effect on synaptic release probability is transient.* (A) Sketch of the experimental procedure and (B) representative traces of pair recordings. In the first row, presynaptic action potentials and below the corresponding unitary eEPSC, recorded 6 min (left) and 18 min (right) after 20 ug/mL s-GO application (for 30 s). (C) The plot summarizes the averaged paired-pulse ratio measured at 6 and 18 min after s-GO treatment. These were respectively 0.76 ± 0.19 and 0.62 ± 0.17 (n=5). *p < 0.05

References

1. G. Di Mauro, R. Amoriello, N. Lozano, A. Carnasciali, D. Guasti, M. Becucci, G. Cellot, K. Kostarelos, C. Ballerini and L. Ballerini, Graphene Oxide Nanosheets Reduce Astrocyte Reactivity to Inflammation and Ameliorate Experimental Autoimmune Encephalomyelitis, *ACS Nano*, 2023, **17**, 1965–1978.
2. S. P. Mukherjee, N. Lozano, M. Kucki, A. E. Del Rio Castillo, L. Newman, E. Vázquez, K. Kostarelos, P. Wick and B. Fadeel, Detection of Endotoxin Contamination of Graphene Based Materials Using the TNF-α Expression Test and Guidelines for Endotoxin-Free Graphene Oxide Production, *PLoS One*, 2016, **11**, e0166816.

3. A. F. Rodrigues, L. Newman, N. Lozano, S. P. Mukherjee, B. Fadeel, C. Bussy and K. Kostarelos, A Blueprint for the Synthesis and Characterisation of Thin Graphene Oxide with Controlled Lateral Dimensions for Biomedicine, *2D Mater.*, 2018, **5**, 035020.
4. A. Franceschi Biagioni, G. Cellot, E. Pati, N. Lozano, B. Ballesteros, R. Casani, N. C. Coimbra, K. Kostarelos and L. Ballerini, Graphene oxide prevents lateral amygdala dysfunctional synaptic plasticity and reverts long lasting anxiety behavior in rats, *Biomaterials*, 2021, **271**, 120749.
5. J. Tejada, K. T. Chaim and S. Morato, X-PloRat: a software for scoring animal behavior in enclosed spaces, *Psic.: Teor. Pesq.*, 2017, **33**, e3322.
6. F. Franceschi Biagioni, R. C. de Oliveira, R. de Oliveira, J. A. da Silva, T. dos Anjos-Garcia, C. M. Roncon, A. P. Corrado, H. Zangrossi, Jr. and N. C. Coimbra, 5-Hydroxytryptamine 1A receptors in the dorsomedial hypothalamus connected to dorsal raphe nucleus inputs modulate defensive behaviours and mediate innate fear-induced antinociception, *Eur. Neuropsychopharmacol.*, 2016, **26**, 532–545.
7. E. L. Louth, C. D. Sutton, A. L. Mendell, N. J. MacLusky and C. D. C. Bailey, Imaging Neurons within Thick Brain Sections Using the Golgi-Cox Method, *J. Visualized Exp.*, 2017, **122**, 55358.
8. W. C. Risher, T. Ustunkaya, J. Singh Alvarado and C. Eroglu, Rapid Golgi analysis method for efficient and unbiased classification of dendritic spines, *PLoS One*, 2014, **9**, e107591.
9. P. Chakraborty and S. Chattarji, Timing is everything: differential effects of chronic stress on fear extinction, *Psychopharmacology*, 2019, **236**, 73–86.
10. R. Mitra, R. Adamec and R. Sapolsky, Resilience against predator stress and dendritic morphology of amygdala neurons, *Behav. Brain Res.*, 2009, **205**, 535–543.
11. Y. E. Wu, L. Pan, Y. Zuo, X. Li and W. Hong, Detecting Activated Cell Populations Using Single-Cell RNA-Seq, *Neuron*, 2017, **96**, 313–329.e6.
12. R. Khazipov, D. Zaynutdinova, E. Ogievetsky, G. Valeeva, O. Mitrukhina, J. B. Manent and A. Represa, Atlas of the Postnatal Rat Brain in Stereotaxic Coordinates, *Front Neuroanat.*, 2015, **9**, 161.
13. G. Cellot, F. M. Toma, Z. K. Varley, J. Laishram, A. Villari, M. Quintana, S. Cipollone, M. Prato and L. Ballerini, Carbon nanotube scaffolds tune synaptic strength in cultured neural circuits: novel frontiers in nanomaterial-tissue interactions, *J. Neurosci.*, 2011, **31**, 12945–12953.
14. R. Rauti, N. Lozano, V. León, D. Scaini, M. Musto, I. Rago Ulloa, F. P. Severino, A. Fabbro, L. Casalis, E. Vázquez, K. Kostarelos, M. Prato and L. Ballerini, Graphene Oxide Nanosheets Reshape Synaptic Function in Cultured Brain Networks, *ACS Nano*, 2016, **10**, 4459–4471.
15. P. Pavlidis, J. Montgomery and D. V. Madison, Presynaptic protein kinase activity supports long-term potentiation at synapses between individual hippocampal neurons, *J. Neurosci.*, 2000, **20**, 4497–4505.